Microwave and Electrostatic Probe Measurements on a Blunt Re-Entry Vehicle

DALLAS T. HAYES* AND WALTER ROTMAN†
Air Force Cambridge Research Laboratories, Bedford, Mass.

The electron density profile on a blunt nosed body has been measured by microwave antennas and electrostatic probes during re-entry and compared with flowfield predictions. The flowfield models assumed a completely viscous layer behind the shock in the stagnation region. In one model the vibrational levels of the molecular species were assumed to be in equilibrium at the gas temperature. This condition was relaxed for the second model. The probes were operated at a high bias to collect the full random current at the sheath edge. The bias was varied in order to measure the electron density at several distances normal to the vehicle surface. The microwave measurements determined signal attenuation, reflection coefficient, and mutual coupling as a function of altitude. At altitudes between 200,000 and 250,000 ft, the viscous flowfield model which assumes vibrational nonequilibrium of the molecular species predicts the electron density over the hemispherical nosecap within an altitude error of less than two thousand feet. This variation is within the limits imposed by the expected diurnal and seasonal changes in the atmosphere.

Nomenclature

A_p = surface area of electrostatic probe
A_f = additional collecting area of probe due to fringing field
e = charge of electron
f_o = operating frequency
f_p = plasma frequency
I_c = convection current to probe
j = current density
k = Boltzmann's constant
m = mass of flowfield specie
n = charged particle density, cm^{-3}
R_N = vehicle nosecap radius
r_p = radius of probe surface
S = distance from nosecap center point, measured along body surface
S' = distance from stagnation point, measured along body surface
T = temperature, °K
U = flow velocity
V = probe bias
v_{th} = thermal speed of flowfield specie
y = normal distance from body surface
ε_0 = permittivity of free space
μ = mobility of charged specie

Subscripts

e, i = property of electrons or ions respectively
s = conditions at edge of probe sheath

Introduction

A SHOCK-IONIZED flowfield is formed about any aerospace vehicle which traverses the upper atmosphere at hypersonic velocities. This ionized flowfield degrades the quality of radio signals transmitted from the vehicle, causing a complete "blackout" in communications under certain re-entry conditions.[1] Numerous attempts have been made to develop a predictive ability for determining the effects of the ionized flowfields upon electromagnetic transmission from aerospace vehicles.[2] In many instances, flight test results are relatively difficult to compare with theory, because of complicating factors such as ablative contamination of the flowfields from heat shield materials or complex body geometry. This paper describes diagnostic re-entry measurements, made on three re-entry flight tests under relatively idealized conditions; i.e., a simple geometry and a clean plasma due to a heat sink, rather than heat shield, design of the nosecap.

The re-entry vehicle used for these tests is a blunt, aluminum hemisphere-cone of 6.33-in. nose radius. The nose cone with the sensor configuration used in the third flight is depicted in Fig. 1. A cutaway side view (with sensors used in the second flight) is shown, together with pertinent dimensions, in Fig. 2. (The sensors and their locations were similar for the first two flights.) A Trailblazer II rocket propelled the nose cone to an apogee of approximately 200 miles. Then the vehicle was accelerated back into the atmosphere along an almost vertical trajectory with a re-entry velocity of 17,500 fps.

The three rockets of this AFCRL diagnostics flight series were launched from the NASA Rocket Launch Facility (Wallops

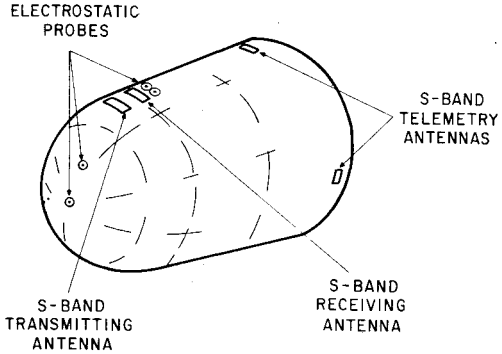

Fig. 1 Trailblazer re-entry vehicle (Flight No. 3).

Received June 21, 1972; presented as Paper 72-693 at the AIAA 5th Fluid and Plasma Dynamics Conference, Boston, Mass., June 26–28, 1972; revision received December 1, 1972. The authors wish especially to thank J. Lennon for the great deal of assistance he provided in performing this study. The basic flowfield calculations were performed under Contract F19628-69-C-0112 by H. Lew of the General Electric Company.

Index categories: Supersonic and Hypersonic Flow; Plasma Dynamics and MHD; Entry Vehicles and Landers.

* Research Physicist, Microwave Physics Laboratory.

† Chief, Plasma Electromagnetics Branch, Microwave Physics Laboratory.

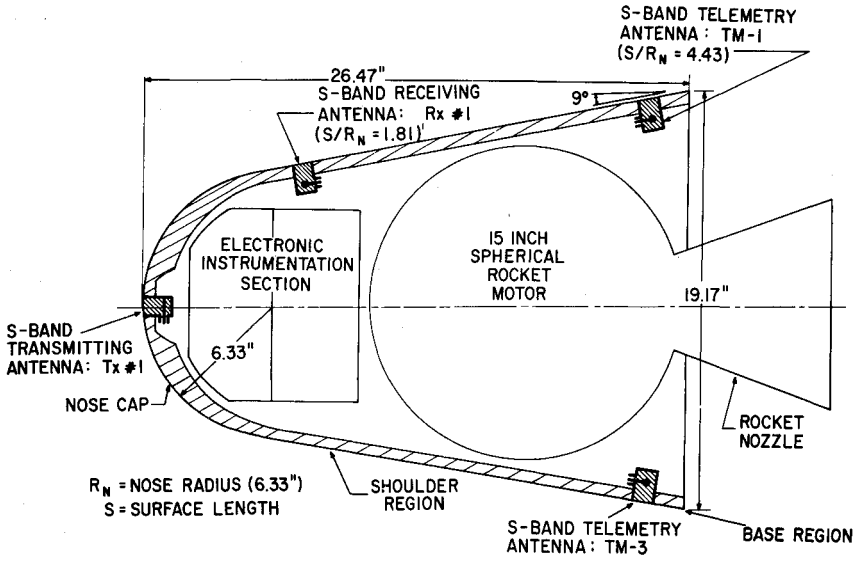

Fig. 2 Location of test and telemetry antennas on nose cone (Flight No. 2).

Island, Va.) in June 1967, June 1969, and October 1970. The payload in each nose cone consisted of several sensors which were designed to measure the ionized flowfield properties during re-entry. Detailed results of these flight tests may be found in Refs. 3–6. This paper is primarily concerned with measurements obtained from S-band microwave antennas on the second flight and electrostatic probes on the third. These were all located on the hemispherical nosecap of the re-entry vehicle. (The response of other probes on the side of the vehicle has been analyzed, but is not discussed here.) Although the region near the stagnation point is not optimum for operational antennas, it is ideal for test purposes because the ability to predict the electrical properties of the flow is greatest in this region. In addition, angle of attack effects, which complicate measurements along the flank, are virtually nil.

Re-Entry Vehicle Instrumentation

The configuration of the two payloads differed mainly in the placement of the diagnostic sensors. The location of the test antennas on the re-entry vehicle for the second flight is shown in Fig. 2. Both the S-band transmitting antenna located at the nosecap center point and the receiving antenna (S/R_N = 1.81) were cavity-backed, probe-fed slot radiators (Fig. 3) designed to operate at a frequency of 2830 MHz.

The instrumentation for the diagnostic measurements on the third flight is indicated in Fig. 1. Each of the four electrostatic probes consisted of a flush-mounted gold plated copper electrode electrically isolated from the vehicle surface (Fig. 4). These were improved versions of electrostatic probes which were flown, with good results, on the first two flights. They were capable of measuring electron densities over a four-decade range and contained circuitry for automatic temperature compensation and preflight calibration.

One probe was located at the nosecap centerpoint ($S/R_N = 0$) and was biased at a fixed voltage of -15 v to collect ion saturation current. In order to measure the ion density at several distances normal to the vehicle surface, the probe bias was varied for the two probes located at $S/R_N = 0.475$ and 2.58 in sequential steps of -5, -15, and -30 v at a rate of 300 cycles per second. Thus, the plasma was sampled ten times at each bias level for each revolution of the vehicle about its center axis. This stepping rate was selected to insure that the plasma conditions would not change appreciably during one cycle (-5 to -30 v). A positive biased probe ($+15$ v), located at $S/R_N = 2.58$, provided a simultaneous measurement of electron saturation current. A microwave transmitting antenna near this

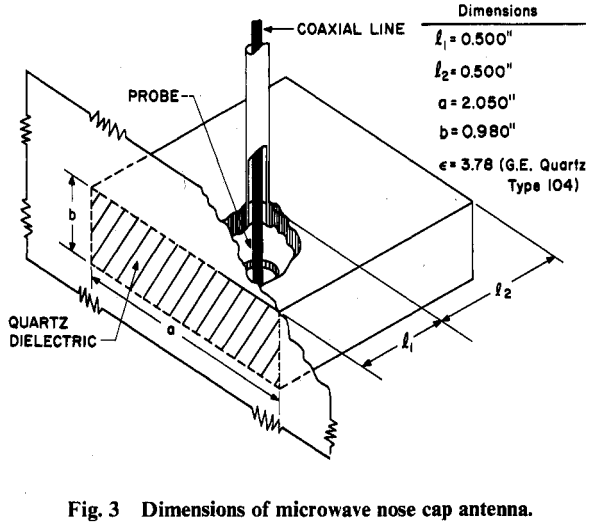

Fig. 3 Dimensions of microwave nose cap antenna.

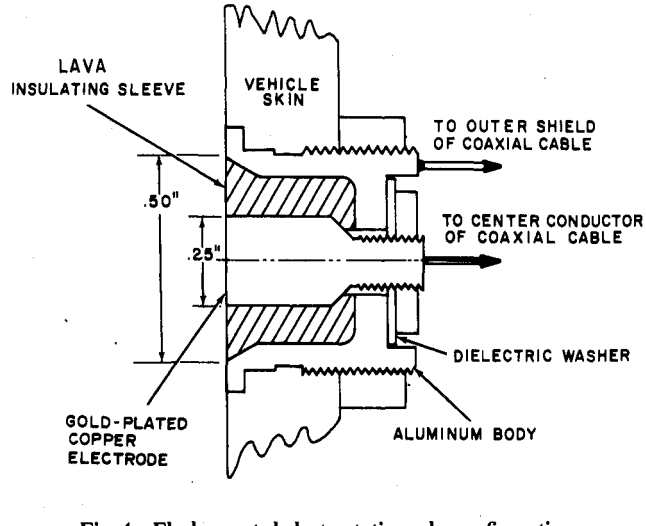

Fig. 4 Flushmounted electrostatic probe configuration.

Table 1 Reaction system and rates

Reaction	Forward rate, cm^3/molesec	Backward rate, cm^3/molesec or $cm^6/mole^2$ sec
$O_2+M \rightleftarrows O+O+M$	$8.74 \times 10^{17} T^{-1.0} \exp(-5.94 \times 10^4/T)$	$7.26 \times 10^{14} T^{-0.5}$
$N_2+M \rightleftarrows N+N+M$	$2.41 \times 10^{16} T^{-1.8} \exp(-1.13 \times 10^5/T)$	$1.34 \times 10^{17} T^{-0.8}$
$NO+M \rightleftarrows N+O+M$	$1.45 \times 10^{16} \exp(-7.54 \times 10^4/T)$	3.63×10^{15}
$O+NO \rightleftarrows N+O_2$	$4.33 \times 10^7 T^{1.5} \exp(-1.81 \times 10^4/T)$	$1.81 \times 10^4 T^{1.5} \exp(-3 \times 10^3/T)$
$O+N_2 \rightleftarrows N+NO$	$6.02 \times 10^{13} \exp(-3.8 \times 10^4/T)$	1.32×10^{13}
$O+N \rightleftarrows NO^+ + e$	$5.18 \times 10^{11} \exp(-3.19 \times 10^4/T)$	$1.44 \times 10^{21} T^{-1.5}$

same location, also, gave additional diagnostic data which aided in the interpretation of the probe measurements. All data obtained from the sensors on the nose cones were telemetered to a ground station by an array of four S-band antennas located at the rear of each vehicle ($S/R_N = 4.35$, Figs. 1 and 2).

Theoretical Analysis

Flowfield Prediction Model

Probe and microwave data from the first flight test[3] for altitudes below 200,000 ft showed adequate agreement with a boundary layer and inviscid flowfield calculation. However, above this altitude there was sharp disagreement. Therefore, a different flowfield model was used to calculate the flowfield properties[7] for the high altitude (>200,000 ft) regime. The air species included in the calculation are N_2, O_2, NO, NO^+ and electrons. The specific reactions and the corresponding rate coefficients[8] are listed in Table 1. For the re-entry velocity of 17,500 fps it was assumed that the only important ionization reaction is

$$N+O \rightleftarrows NO^+ + e$$

The production of other ions (such as O_2^+) is unimportant at re-entry velocities less than 20,000 fps.

In these calculations the flowfield in the stagnation region of the vehicle was not divided into a boundary layer and an inviscid flow regime but, rather, was considered to be viscous from the body out to the shock. A model was used whereby the effects of heat conduction, shear stress, and diffusion were present at the shock front. Chemical equilibrium of the high temperature air behind the shock was not assumed. However, the vibrational and rotational excitation of molecular species were first assumed to be in equilibrium. The effect of viscosity prevailing over the entire shock layer region was evident in the results. The maximum temperature was obtained in all cases near the shock interface. However, due to diffusion, the peak electron density and atomic species concentration occurred somewhere within the viscous layer and not at the edge where the maximum production takes place. A five order of magnitude change of peak electron density was predicted over the altitude range from 270,000 ft down to 200,000 ft. Sample electron density profiles calculated using this program are shown in Fig. 5.

The additional assumption of vibrational nonequilibrium has two consequences in the stagnation region. First, the kinetic temperature is raised over that of the vibrational equilibrium case as the heat capacity of the gas is only a portion of the vibrational equilibrium value. Second, the rate of dissociation of N_2 is slowed down. These two effects compete in the production of electrons. For a re-entry velocity of 17,500 fps the calculations show (Fig. 6) that the slower production rate of N and O predominates at 270,000 ft, resulting in a lower peak electron density by a factor of approximately eight over the vibrational equilibrium case. At 240,000 ft the higher kinetic temperature predominates and the electron density is increased by a factor of 2.5. However, at 200,000 ft the assumption of vibrational nonequilibrium results in the prediction of a peak electron density which is only 50% greater than the vibrational equilibrium case.

The collision frequency profiles are relatively uniform across the shock layer and, in contrast to the electron density, are not greatly affected by the vibrational nonequilibrium assumptions, typically differing by only a few percent from the equilibrium case.

The electron density, which is present in the flowfield only as a trace specie, can be very sensitive to the rate constants chosen for the production and loss of electrons. To determine this sensitivity the rate constant for the dissociative recombination of the electrons with NO^+ was arbitrarily dropped by an order of magnitude and the electron density at the stagnation point for an altitude of 240,000 ft was calculated. The peak electron density predicted was 3.32×10^{11} el/cm^3. This is a negligible change from the value of 3.22×10^{11} el/cm^3 obtained using the rate constant given Table 1 for this reaction. Since the measured electron density is expected at the best to be accurate only to within a factor of two, no further consideration was made of the uncertainty in reaction rate constants.

The requirement for a completely viscous solution is relaxed

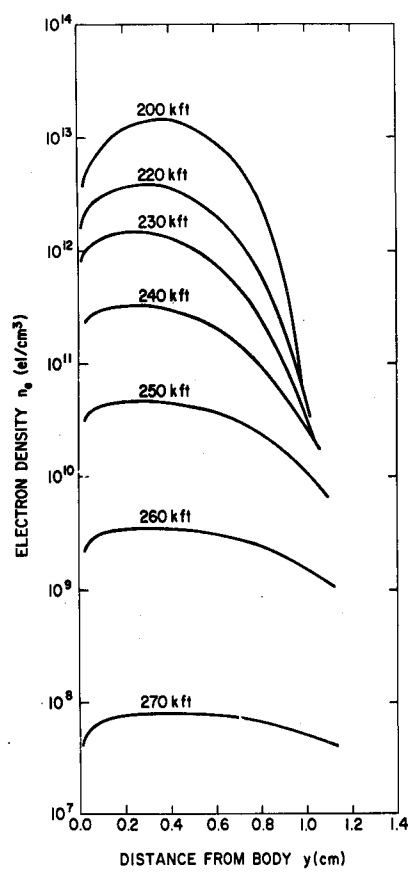

Fig. 5 Electron density profiles in the stagnation region calculated assuming vibrational equilibrium of the molecular species.

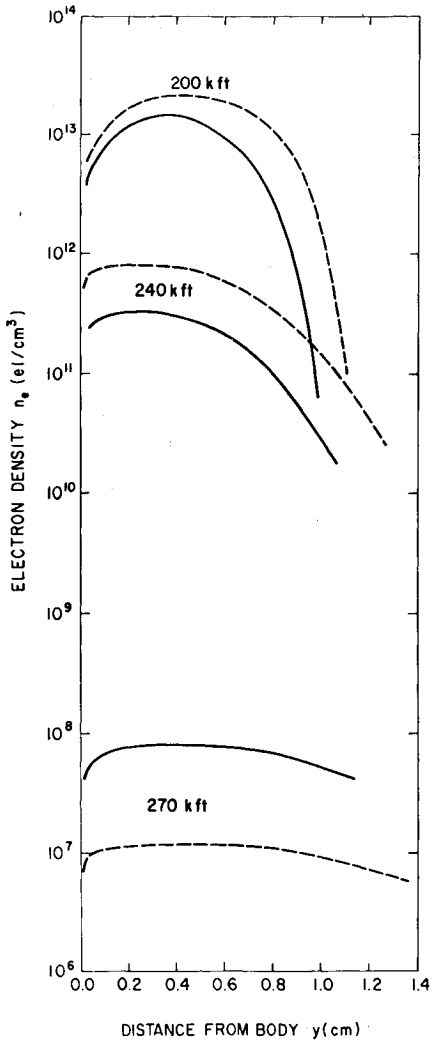

Fig. 6 Comparison of the vibrational equilibrium electron density profiles (——) with those calculated assuming vibrational non-equilibrium (- - - -).

in the flow along the body away from the stagnation point. The equations of motion for a chemically reacting flow along inviscid streamlines are integrated and the mass flux at a given location is matched to that of the local boundary layer. The edge conditions resulting from this match are then used in a solution of the viscous laminar boundary-layer equations. Details of the method are given in Ref. 9.‡

Electrostatic Probe Theory

The analysis of electrostatic probes which are flush-mounted on a hypersonic re-entry vehicle is complicated if one desires to obtain a general solution relating the current collected by the probe to the properties of the flowfield. In the inhomogeneous plasma layer formed around the vehicle the electron density increases from a low value close to the vehicle surface to a maximum somewhere in the boundary layer and then decreases with distance into the laminar flow region. The low electron density close to the vehicle surface results in a large Debye length in this region. In general, this means that the mean free path is less than the sheath thickness so the effect of collisions in the sheath must be included in the analysis. Also, if the probe bias is high, the probe sheath may extend far enough into the boundary layer so that the effect of convection must be included. In addition, the collecting area of the probe may become appreciably different from the actual physical area of the probe when the sheath thickness becomes of the order of the probe dimensions.

For accurate results the flowfield equations discussed in the previous section, must be solved simultaneously with the electromagnetic equations describing the interaction of the probe's electric fields with the flowfield. However, adequate results can be obtained from a relatively simple theory first proposed by Bredfeldt and Scharfman[10] to correlate the collected current with the electron density at a discrete point in the flowfield as a function of altitude. Here, it is assumed that the sheath thickness is small compared with the boundary-layer thickness so that convective effects may be neglected and that the sheath collecting area is equal to the physical area of the probe surface. The full random flux of ionized particles of one sign is assumed to be collected by the probe, i.e.,

$$j = 1/4nev_{\text{th}} \tag{1}$$

The planar, space-limited, mobility-controlled diode equation

$$j = 9/8\varepsilon_0\mu_s(V^2/y_s{}^3) \tag{2}$$

is then used to locate the sheath edge. Following Bohm,[11] the electron temperature is used in calculating the thermal speed of collected particles at the sheath edge

$$v_{\text{th}} = (3kT_e/m)^{1/2} \tag{3}$$

The assumption that the full random current is collected is reconcilable with the fact that the sheath is collision dominated only if the ionized particles are not scattered out of the sheath in collisions with neutral particles. This is most probably the case when the energy imparted to the ionized particle by the sheath field per mean free path is greater than the thermal energy of the particle. In shock tunnel measurements Scharfman and Bredfeldt[12] have shown that for negative biases less than -15 v the positive ion density at the edge of the sheath could be measured to within a factor of two. However, the validity of this simple theory is doubtful when applied for electrons, which are scattered at large angles due to their light mass relative to the neutral particles with which they collide in the sheath. The probability that an electron will be scattered out of the sheath region and not be collected by the probe is high compared to that for ions being collected by a probe biased negatively at the same magnitude. The validity of this theory under conditions where electrons are collected was evaluated for the flight data by comparing the response of the positively biased probe ($+15$ v at $S/R = 2.58$) with a similarly located, negatively biased probe for positive ion collection. The measured electron density agreed within a factor of three with the positive ion density for all measurements made below 250,000 ft.

In reducing the data the dominant neutral specie in the flowfield was assumed to be N_2 and the dominant ionized specie NO^+. The simplest kinetic theory expression for the mobility was used. The pressure and temperature were obtained from flowfield predictions. The pressure presented no difficulty—being constant across the boundary layer at any altitude. However, the temperature varies rapidly in the boundary layer. An appropriate value was determined by an iterative procedure in which the local temperatures, corresponding to different heights in the flow, were selected until a sheath thickness, consistent with its temperature, was found.

Two factors which might invalidate this probe theory are the increased current to the probe caused by an enlarged sheath area and the convection from the flowfield into the sheath region. The magnitude of their effect now will be examined theoretically and later included in the analysis of the data. A rough estimate of the increased current due to an enlarged sheath area can be obtained by assuming that this area is given by the physical area of the surface of a 90° cross-sectional segment of a torus bordering on the perimeter of the probe

$$A_f = \pi^2 r_p y_s + 2\pi y_s{}^2 \tag{4}$$

‡ At the time of this writing the only calculations which have been extended around the body are those assuming vibrational equilibrium in the stagnation region.

The ratio of the total probe collecting area to its surface area is

$$C = (A_p + A_f)/A_p = 1 + \pi(y_s/r_p) + (y_s/r_p)^2 \quad (5)$$

To estimate the effect of convection it is assumed that all current flowing into the sheath volume from the upstream direction would be collected. Thus

$$I_c = en_{is} U_s (A_f/2) \quad (6)$$

Equation (6) assumes the convective velocity and electron density over the entire collecting area to be given by their maximum value at the edge of the sheath. It is thus an upper bound on the magnitude of the convective current.

The probe results serve to identify the local plasma properties. A second type of flight data, which is obtained from microwave measurements, involves the effect of the entire plasma profile. The two measurements thus complement each other.

Microwave Antenna Model

The effects of the plasma sheath upon the performance characteristics of the microwave test antenna of the second flight will now be considered. The basic parameters required from the flowfield models are the electron density and collision frequency profiles at the stagnation point of the nose cone. These profiles were used as inputs to a computer program[13] which derives theoretical power reflection coefficient and radiated signal strength curves for an open-ended waveguide in a ground plane which is covered by a homogeneously layered, plasma medium. The pertinent inputs to the program consist of the following: a) the numbers of layers of the specified plasma model, b) the electron density and collision frequency of each layer, c) the distance of each layer from the ground plane, d) the frequency (S-band, 2830 MHz), and e) the cross-sectional dimensions of the rectangular waveguide (2.05 in. × 0.98 in.). Since the test antenna is a cavity-backed, probe-fed slot radiator (Fig. 3) rather than an open-ended waveguide, the computed admittance at the aperture of the antenna must be converted into the input admittance and reflection coefficient at the coaxial input. This transformation is accomplished by the use of an equivalent network[3] which represents the physical dimensions§ of the test antenna.¶ The results of the theoretical analysis can then be compared directly with the flight test data. The use of the theoretical antenna model requires some justification since the nose cap antenna is located on the hemispherical surface of a complex structure while the analysis assumes a flat ground plane. Theoretical calculations show that the input admittance of the test antenna, under freespace conditions, is almost exactly the same whether it is mounted in a flat ground plane or on a cylindrical surface (longitudinal slots) of the same radius (6 in.) as the hemisphere of the nose cone. The mutual coupling to a second antenna (E-plane coupling), on the other hand, depends strongly upon whether the ground plane is flat or cylindrical. These same relative effects are also found when the ground plane is covered with a plasma sheath.[14]

The measured freespace radiation patterns of the test antenna on the nose cone are almost identical in the forward region ($\pm 60°$ from the body axis of the nose cone) to those with the antenna on a flat ground plane but, of course, are greatly different in the rearward and broadside regions. This result is expected theoretically[15] from the radiation patterns of a slot antenna on a spherical surface which is several wavelengths in diameter. The flat ground plane computer model may therefore be expected to predict antenna self-admittance (reflected power) and radiated power into the forward region from the nose cone, while mutual coupling effects and radiation in other directions require additional consideration. Fortunately, the ground receiving stations were located in the forward direction (less than 50° from body axis) for the re-entry portion of the trajectory so that received signal intensity could be compared directly with computer results.

§ Two parameters in the equivalent network are determined from the imposed condition that the antenna be matched under freespace (no plasma) conditions.

¶ An alternative approach to the use of an equivalent network which is based upon the physical dimensions of the antenna is a network representation in the form of the *ABCD* transformation matrix. The latter approach has the advantage that the elements of the *ABCD* matrix may be determined directly from external measurements on the antenna and does not require that the antenna be initially matched to some specified condition.

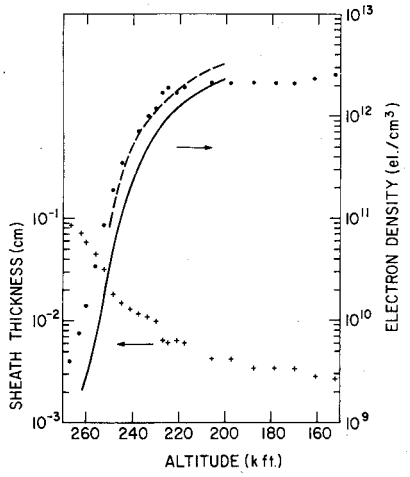

Fig. 7 Comparison of electron density (·) measured by nosecap centerline probe, with predictions of vibrational equilibrium (——) and nonequilibrium (----) flowfield models. (+ denotes measured sheath thickness.)

Results and Discussion

Electrostatic Probes

Fixed negative bias probe ($S/R_N = 0$)

Since the vehicle re-entered at an angle of attack of 10° on the third flight, the stagnation point was displaced from the position of this probe by an amount $S'/R = 0.175$. The probe was biased 15 v negative to collect ion saturation current. Figure 7 shows the charged particle density vs altitude using Eq. (2). The positive ion density, which the probe actually measures, and the electron density are assumed to be equal in this graph since the negative ion density (e.g., O^-, O_2^-) is most likely negligible. The local ion density must, therefore, be equal to the electron density from charge neutrality considerations. In the lower part of this figure is the calculated sheath thickness (designated by +) obtained from the probe current using Eq. (1). This curve gives the normal distance (y_s) from the probe surface at which the ion density for a particular altitude was measured. The sheath thickness values were then used to select, from the curves of Figs. 5 and 6 the theoretical electron density values calculated at this same height above the vehicle surface. These results are compared in Fig. 7 with the probe measurements as a function of altitude.

At altitudes above 220,000 ft the vibrational equilibrium calculation is less than the measured values by a factor of two or more. The disagreement becomes increasingly worse at the higher altitudes, as would be expected since the assumption of vibrational equilibrium is less valid at lower gas pressures. On the other hand, the electron densities from the nonequilibrium calculations (also shown in Fig. 7) agree remarkably well with the flight data up to altitudes of 250,000 ft.

At 270,000 ft (not shown in Fig. 7), the discrepancy is even larger between measured and theoretical electron density. The vibrational equilibrium calculation which is the higher value at this altitude predicts an electron density $\sim 7 \times 10^7$ el/cm^3 while the measured value is $\sim 3 \times 10^9$ el/cm^3. Calculations of the sheath thickness for this altitude show $y_s/r_p \approx 0.3$. Thus it is quite possible that the actual sheath area is much greater than the probe area. It is also possible that the convection

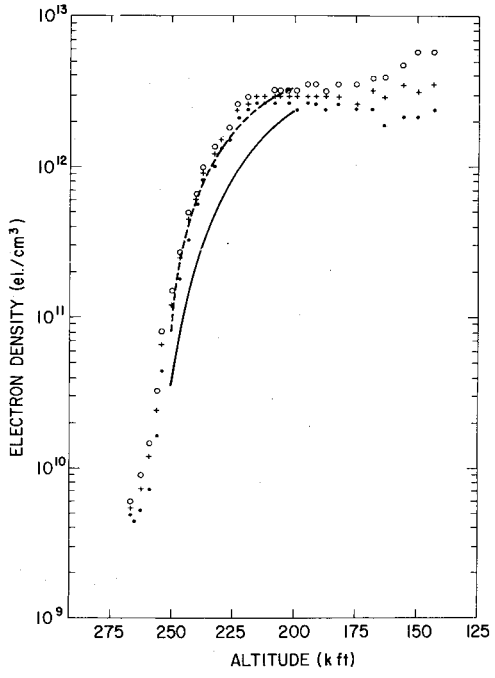

Fig. 8 Comparison of electron density measured by variable bias probe on windward side ($S'/R_N = 0.3$) with predictions of vibrational equilibrium (——) and nonequilibrium (----) flowfield models. (·, +, ◦ denote electron densities measured at −5 v, −15 v, −30 v probe bias, respectively.)

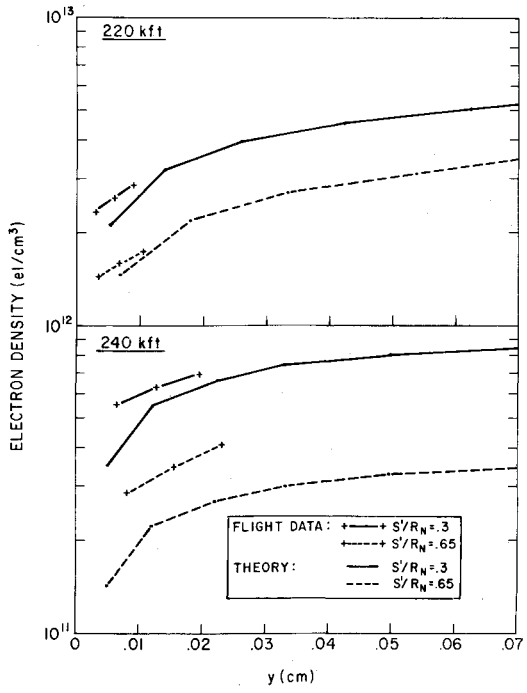

Fig. 9 Electron density profile in nose cap region measured by variable bias probe (windward side, $S'/R_N = 0.3$, leeward side, $S'/R_N = 0.65$).

current into the probe is an appreciable portion of the collected current.

Equation (5) has been used to estimate the effects of fringing fields. At 270,000 ft (where $y_s \approx 0.1$ cm) one obtains an area correction factor C of 2.2. The fringing fields then reduce the probe current by at most a factor of two. This would not account for the discrepancy of 1.6 orders of magnitude.

An approximate flow velocity was taken from the theoretical calculations to estimate the effect of convection. The corresponding convection current I_c is then obtained from Eq. (6) as about 0.1 μa. This is a negligible quantity, compared to the measured current of 6.13 μa. Thus, fringing fields and convective effects cannot explain the discrepancy between the measured electron density and the predicted value at 270,000 ft.

Variable negative bias probe ($S/R_N = 0.475$)

The nonzero angle of attack and spin of the vehicle (11 rev/sec) caused the probe at $S/R_N = 0.475$ to sample the current from the ionized flowfield at $S'/R_N = 0.30$ on its windward side and at $S'R_N = 0.65$ on the leeward side (measured relative to the stagnation point). Figure 8 shows a comparison between the electron density measured at each of the three bias levels on the windward side of the vehicle and the theoretical electron density computed from the vibrational equilibrium model. Corresponding vibrational nonequilibrium values were obtained at altitudes below 260,000 ft by shifting the equilibrium values upward by the ratio of the electron densities in the stagnation region, as predicted from the two models. This procedure probably gives a good estimate of the vibrational nonequilibrium effects since the probe is always relatively close to the stagnation point (within 2 in.). The flight test data show excellent agreement with the predictions of the vibrational nonequilibrium model, similar to the previous case for the on-axis ($S/R_N = 0$) probe.

Similarly, poor agreement was obtained with the predicted value of the electron density at 270,000 ft (using the vibrational equilibrium model). The effects of fringing fields and convection were likewise estimated to be negligible (as was the case for the on-axis probe at $S'/R_N = 0.175$). The reason for this discrepancy remains unresolved.

Since this is a variable bias probe, the current as a function of probe bias measures the electron density over a range of values of y. Figure 9 compares the measured values of electron density on the windward and leeward sides with the predicted vibrational nonequilibrium profiles (estimated from the equilibrium values, as in Fig. 8) at altitudes of 220,000 and 240,000 ft. The slope of the measured electron density curves is seen to agree with the predicted profiles in all cases.

It should also be noted that the probe is sampling the charged particle density almost out to the region where the density has reached its peak value. In the worst case (220,000 ft) the peak electron density is only a factor of two greater than the density measured by the probe at $y = 0.01$ cm (30 v bias). Thus, it is permissible to compare probe data for these altitudes to the microwave data which is sensitive primarily to the peak electron density in the profile.

Microwave Measurements

Power Reflection Coefficient

The microwave parameters, measured for the nose cap antenna on the second Trailblazer rocket flight, include reflected power, signal intensity at a ground receiving station, and mutual coupling to a second identical antenna located at the shoulder of the nose cone. The measured reflection coefficient at the terminals of the nose cap antenna (Fig. 10) increases sharply from essentially zero (freespace value) at an altitude of 260,000 ft, where the received signal at the ground stations begins to decrease, to almost one hundred percent (total reflection) by 240,000 ft. Figure 10 also shows the theoretical variation of the reflection coefficient for the two flowfield models. The vibrational equilibrium results have essentially the same rate of increase with descending altitude as the flight data, but occur ten thousand feet lower in altitude. Excellent agreement is obtained when the vibrational nonequilibrium calculations are used to predict the reflection coefficient. Here, the altitude at which the predicted onset of plasma effects and the subsequent increase of reflected power agrees with the measurement to within 2000 ft. This altitude difference is only slightly greater than that expected

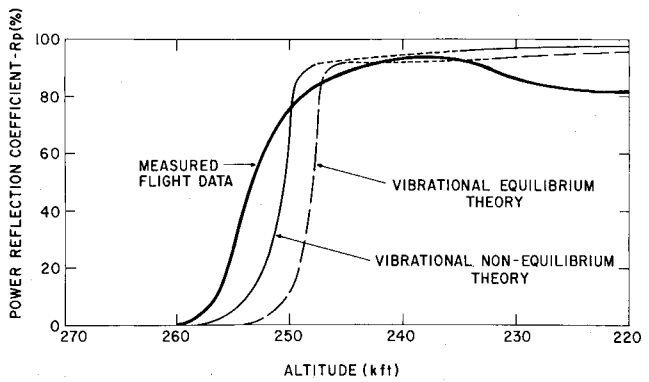

Fig. 10 Comparison of theoretical and measured power reflection coefficient for nose cap antenna (region of plasma resonance shown as dashed lines).

from seasonal and diurnal variations in atmospheric parameters.[16]

Received Signal Intensity

The same general correlations with flowfield predictions are observed for the received signal intensity at the ground station (Fig. 11). The measured intensity is practically constant down to an altitude of 260,000 ft below which it decreases rapidly by more than 20 db within an altitude range of 20,000 ft. The vibrational equilibrium curve has the same slope as the flight data, but predicts that the signal decrease should occur almost 10,000 ft lower in altitude. The vibrational nonequilibrium model gives even better agreement in that it reduces this altitude error to 5000 ft.

Detailed calculations with the theoretical models indicate that an anomalous dip in received signal intensity occurs when the electron density n_e reaches the critical value

$$f_o = f_p \equiv 8.93 \times 10^3 (n_e)^{1/2} \text{ el/cm}^3 \qquad (7)$$

This phenomenon has the typically short duration which is characteristic of all the flight plasma transition regimes and is restricted to a 5000-ft range in altitude. The decrease is caused not by any substantial changes in the power reflected or absorbed by the plasma, but rather by the narrowing and subsequent broadening of the antenna radiation pattern at plasma resonance. The beam narrowing concentrates the radiated power in the forward direction of the nose cone, thereby reducing the

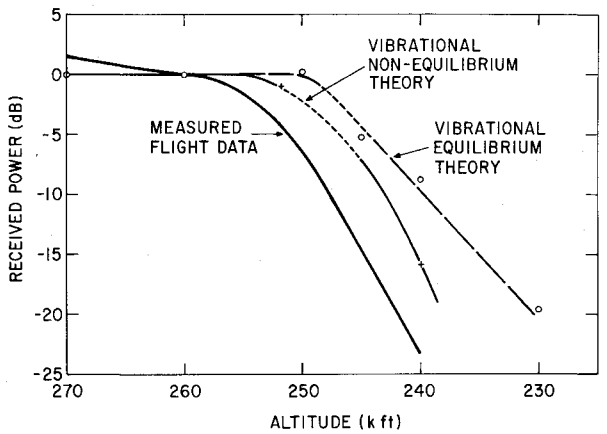

Fig. 11 Comparison of theoretical and measured received signal intensity at ground station for nose cap antenna (region of plasma resonance shown as dashed lines).

received signal at ground stations which are located toward the side of the flight path.

The regions where these transient resonant reductions in signal strength and corresponding small changes in reflected power are expected to occur are shown as the broken lines on the two theoretical curves for both Figs. 10 and 11. The absence of any indication of this resonance effect during flight may be attributable to the low rate of data sampling for the experimental curve where only the results at low transmitter power levels could be used.** Given the short time in which this effect would have been present, it may well have occurred when the transmitted power was sufficiently intense to alter the electrical characteristics of the plasma and destroy the resonance condition.

Confidence in the accuracy of these flight observations is strengthened by the self-consistency between the flight test results. The measured signal intensity is directly proportional to a transmission coefficient which is obtained from the reflection data by simply subtracting the reflected power from the power incident on the antenna. This result is predictable for a thin plasma sheath[17] at high altitudes, where plasma absorption or changes in the shape of the radiation pattern caused by the effect of the plasma medium are small. (However, the analytical conditions for the thin plasma sheath approximation are not satisfied during plasma resonance.) The validity is further reinforced by comparisons with measured antenna radiation patterns and mutual coupling to a second antenna on the side of the nose cone.

Mutual Coupling

The measured mutual coupling, normalized (zero decibels) to freespace conditions, is compared in Fig. 12 with the values which

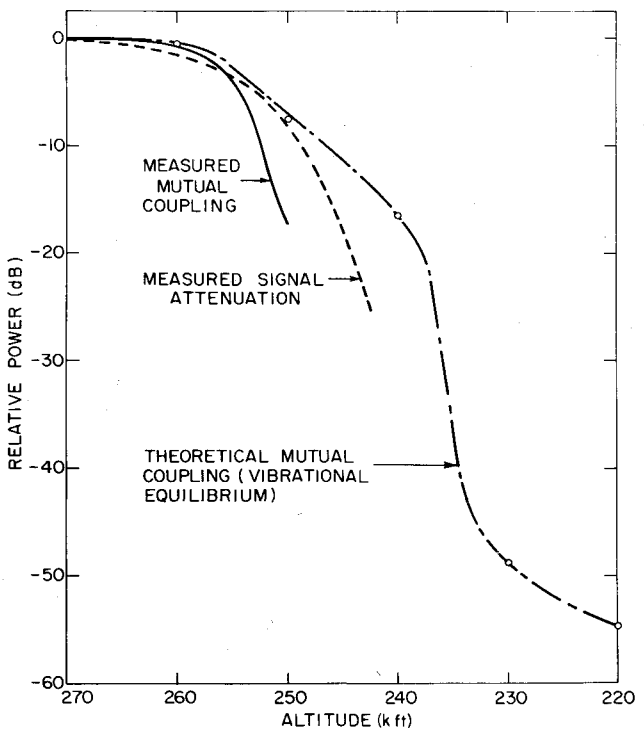

Fig. 12 Comparison of antenna mutual coupling with received signal intensity.

** The S-band output of the test transmitter consists of pulses of 7-μsec duration which were switched during the flight between low (60 w), medium (300 w), and high (600 w) power levels. All test data presented in this paper were recorded only during the low power intervals where the plasma presumably acted as a linear medium.

are computed from electron density profiles at the stagnation point for the vibrational equilibrium flowfield model. The flight data show a rapid decrease in mutual coupling which starts at an altitude of 260,000 ft, similar to the results for received signal intensity and reflected power. The theoretical mutual coupling also shows an intial decrease at 260,000 ft, but deviates considerably from the measurements at lower altitudes. This deviation is not unexpected for several reasons. First, as discussed previously, the theoretical mutual coupling model assumes that the two antennas are located on a flat ground plane whereas they are actually mounted on the curved body of the nose cone. This factor alone results in a difference in coupling of more than ten decibels, even under freespace conditions. Second, the model assumes that the electron density profiles remain unchanged in the region between the two antennas, whereas there was a variation of almost two orders of magnitude between the nose cap and shoulder antennas. Since these factors are not taken into account in the analysis, any agreement between mutual coupling theory and flight data is purely fortuitous.

As a result of this variation in electron density there was a limited range of altitudes during which the nose cap antenna was strongly affected by the plasma while the shoulder antenna was essentially in a freespace environment. If under these restricted conditions the plasma was also assumed to be a thin layer, then the mutual coupling and radiated signal strength would both be proportional to the terminal voltage at the antenna aperture. Therefore they would both be interrelated and should undergo identical variations with altitude. This correlation is observed in Fig. 12 where the measured mutual coupling and signal attenuation (received signal attenuation) both exhibit the same rapid decrease in intensity, beginning at an altitude of 260,000 ft.

Conclusions

At altitudes between 200,000 and 250,000 ft, the viscous flowfield model which assumes vibrational nonequilibrium of the molecular species predicts the electron density over the hemispherical nosecap within an altitude error of less than 2000 ft, as shown by the simultaneous microwave and electrostatic probe data. This variation is within the limits imposed by the expected diurnal and seasonal changes in the atmosphere. The vibrational equilibrium flowfield calculations, on the other hand, predict the correct trends in changes of electron density with an altitude error of ten thousand feet. Both theoretical models give essentially identical results at altitudes below 200,000 ft whereas, at 270,000 ft and above there is an unexplained discrepancy of almost two orders of magnitude between the measured and theoretical electron densities. These results indicate the range of validity of specific flowfield theories for a blunt re-entry vehicle with a velocity of 17,500 fps and may serve as a guide, through scaling laws, for other body shapes and velocities.

References

[1] Rybak, J. P. and Churchill, R. J., "Progress in Reentry Communications," *IEEE Transactions, Aerospace and Electronic Systems*, Vol. AES-7, No. 5, Sept. 1971, pp. 879–894.

[2] Huber, P. W., Evans, J. S., and Schexnayder, C. J., "Comparison of Theoretical and Flight-Measured Ionization in a Blunt Body Re-Entry Flowfield," *AIAA Journal*, Vol. 9, No. 6, June 1971, pp. 1154–1162.

[3] Poirier, J. L., Rotman, W., Hayes, D. T., and Lennon, J. F., "Effects of the Reentry Plasma Sheath on Microwave Antenna Performance: Trailblazer II Rocket Results of 18 June 1967," Rept., AFCRL-69-0354, Aug. 1969, Air Force Cambridge Research Labs., Bedford, Mass.

[4] Rotman, W. and Maloney, L. R., "High Power Microwave Antenna Performance in the Stagnation Region of a Blunt Reentry Nose Cap," Rept. AFCRL-73-0072, Jan. 1973, Air Force Cambridge Research Labs., Bedford, Mass.

[5] Lustig, C. D. and Hayes, D. T., "Observations of Electroacoustic Resonance in a Reentry Sheath," *Proceedings of the IEEE*, Vol. 57, May 1969, pp. 800–802.

[6] Hayes, D. T., Poirier, J. L., and Scharfman, W. E., "The Trailblazer II Reentry Rocket Test Program," *Proceedings of the Anti-Missile Research Advisory Council Meeting*, Vol. 18, Part I, Infrared Physics Lab., Willow Run Labs., Inst. of Science and Technology, Univ. of Michigan, 1968, pp. 479–501.

[7] Lew, H. G., "Shock Layer Ionization at High Altitudes," (Final Rept. on Contract F19628-69-C-0112), AFCRL-70-0702, GE 70SD782, Nov. 1970, The General Electric Co., Valley Forge, Pa.

[8] Bortner, M., "Review of Rate Constants of Selected Reactions of Interest in Reentry Flow Fields in the Atmosphere," T.N. 484, May 1969, Nation Bureau of Standards, Washington, D.C.

[9] Lew, H. G., "Nonequilibrium Blunt Body Flow with Material Ablation," GE 69SD760, July 1969, The General Electric Co., Valley Forge, Pa.

[10] Bredfeldt, H. R., Scharfman, W. E., Guthart, H., and Morita, T., "Boundary-Layer Ion Density Profiles as Measured by Electrostatic Probes," *AIAA Journal*, Vol. 5, No. 1, Jan. 1967, pp. 91–98.

[11] Bohm, D., Burhop, E. H. S., and Massey, H. S. W., "Use of Probes for Plasma Exploration," *The Characteristics of Electrical Discharges in Magnetic Fields*, edited by A. Guthrie and R. K. Wakerling, McGraw-Hill, New York, 1949, Chap. 2.

[12] Scharfman, W. E. and Bredfeldt, H. R., "Experimental Studies of Electrostatic Probes for the Re-entry Measurements Program-Phase B," Subcontract 6-1603 under Prime Contract 30-069 AMC-333 (Y), SRI Project 6138, July 1967, Stanford Research Inst., Menlo Park, Calif.

[13] Fante, R. L., "Reentry Antenna Test (RANT) Program: Linear Antenna Model," Final Report AVSD-0374-69-CR (Contract F04701-68-C-0283), Vol. 2, March 1971, Avco Corp., Wilmington, Mass.

[14] Stewart, G. E. and Golden, K. E., "Self and Mutual Admittance for Axial Slots on a Cylinder in the Presence of an Inhomogeneous Plasma Layer," Rept. TR-0059 (6222-10)-5, (Contract F04701-70-C-0059) Jan. 1971, Aerospace Corp., Los Angeles, Calif.

[15] Cohn, S. B. and Morita, T., "Microwave Radiation from Large Finite Bodies," TR No. 48 (Contract AF19(604)-1296), Jan. 1955, Stanford Research Inst., Stanford, Calif.

[16] Groves, G. V., "Seasonal and Latitudinal Models of Atmospheric Temperature, Pressure, and Density, 25 to 110 Km," Rept. AFCRL-70-0261, May 1970, Air Force Cambridge Research Labs., Bedford, Mass.

[17] Fante, R. L., "Effect of Thin Plasmas on an Aperture Antenna in an Infinite Ground Plane," *Radio Science*, Vol. 2 (New Series: No. 1), Jan. 1967, pp. 87–100.